Object-based classification approach for greenhouse mapping using Landsat-8 imagery

Wu Chaofan, Deng Jinsong, Wang Ke*, Ma Ligang, Amir Reza Shah Tahmassebi

(*Institute of Applied Remote Sensing & Information Technology, Zhejiang University, Hangzhou 310058, China*)

Abstract: Suburban greenhouses with intensive agricultural productivity have increasingly influenced the daily diet and vegetable supply in Chinese cities. With their enormous input of fertilizers and pesticides, greenhouses have considerably changed the local soil quality and environmental risk factors. The ability to obtain timely and accurate information regarding the spatial distribution of greenhouses could make an important contribution to local agricultural management and soil protection. This paper attempts to present a practical framework for extracting suburban greenhouses, integrating remote sensing data from Landsat-8 and object-oriented classification. Inheritance classification was implemented, and various properties, including texture and neighborhood features in addition to spectral information, were investigated through the popular random forest technique for feature selection prior to SVM classification to improve the mapping accuracy. The results demonstrated that object-based classification incorporating non-spectral features yielded a significant improvement compared with the classification results obtained using only the spectral information in traditional per-pixel classification. Both the producer's and user's accuracy were higher than 85% for greenhouse identification. Although it remained a challenge to completely distinguish greenhouses from sparse plants, the final greenhouse map indicated that the proposed object-based classification scheme, providing multiple feature selections and multi-scale analysis, yielded worthwhile information when applied to a continuous series of the freely available Landsat-8 imagery data.

Keywords: greenhouse, mapping, Landsat-8, object-based classification, feature selection, multi-scale

DOI: 10.3965/j.ijabe.20160901.1414

1 Introduction

Beginning in the 1970s, the greenhouse has a history of more than 40 years of rapidly increasing use in China.

Greenhouses appear most commonly in suburban districts as a result of rapid urbanization and the urban population explosion, modifying the characteristics of seasonal agricultural production, reshaping the landscape, and even changing the local climate. As reported by the national State Statistics Bureau, the entire country of China contained 81 000 hm^2 of greenhouses as of 2006. The total greenhouse area worldwide reached 36 5760 hm^2 in 2010, of which China accounts for 42.8%. The remarkable increase in the use of greenhouses reflects the development of modern agriculture, and the increasing rates of greenhouse production are gradually changing the daily lives of inhabitants. Simultaneously, the expansion of greenhouses is exerting controversial effects on the environment, such as soil degradation[1] and vegetable and plastic waste[2]. Furthermore, the greenhouse poses new challenges in land-use planning, as

greenhouse regions can be confused with construction lands in certain cases.   As a result, a reliable method for determining the number and spatial distribution of greenhouses from remote sensing imagery would contribute to land-use planning and agricultural management.

As a prompt and effective technique, remote sensing is playing an increasingly important role in land-use mapping.   Among the operating remote sensing satellites, the Landsat satellites (NASA, National Aeronautics and Space Administration) have produced a series of images for longer than 40 years that are widely applied in land cover classification[3-7].   To address the special case of greenhouses, Li et al.[8] created a greenhouse index for the extraction of greenhouses used as vegetable fields from TM (Thematic Mapper) images in 2004.   Ma[9] used Landsat 5 TM data combined with additional information to perform an SVM (Support Vector Machine) classification of vegetable greenhouses.   Both studies were conducted based on images of 30-meter resolution using the traditional per-pixel classification approach, and they achieved reasonable accuracy using Landsat data, which encouraged further research into applications using 15 m fused imagery.

An increasing number of studies are being conducted on the topic of greenhouse identification via remote sensing based on multiple types of imagery in addition to Landsat data worldwide.   Carvajal et al.[10] compared different high-resolution satellite images (e.g., QuickBird and IKONOS) in a study of greenhouse detection in Southeastern Spain.   DilekKoc-San et al. compared the application of different classification techniques to WorldView-2 satellite imagery for the detection and discrimination of plastic and glass greenhouses[11].   An object-based classification scheme was applied by Tarantino et al.[12] to identify plastic-covered vineyards from true-color aerial data.   Agüera performed greenhouse delineation through maximum likelihood classification and completed the extraction and classification of homogeneous objects combined with calibration and pseudo-calibration using images from the QuickBird and IKONOS satellites[13].

On the one hand, all of these greenhouse detection studies were generally conducted on high-resolution images, providing many object details.   On the other hand, such images are acquired at higher cost, offer narrower spatial coverage and are less readily available than the latest Landsat-8 imagery, which offers a 15 m panchromatic band, is currently freely downloadable as a continuous record of 41 years of earth observations and offers novel opportunities for classification[14], especially for developing countries with rapid greenhouse growth, such as China.

In recent decades, improvements in the resolution of satellite images as well as the popularization and advancements in software have made object-based classification a priority[15].   Compared with traditional per-pixel classification, in which different objects are predominantly classified based on spectral features, object-oriented classification offers the following advantages: the classification is based on objects represented by combinations of several similar pixels rather than on single pixels to avoid the salt-and-pepper effect; instead of a single scale, multiple scales of vertically connected (super-objects and sub-objects) and horizontally connected (neighbor objects) heritance relationships can be used to optimize the classification process; and the spatial relationships, textural properties and contextual information of objects in addition to the traditional spectral characteristics are all attractive features for classification[16,17].

A multitude of papers have utilized Landsat data for the application of object-based classification[18-22].   However, there are few papers concerning such applications for greenhouse classification, and in particular, there has been no research on greenhouse classification utilizing Landsat-8 imagery.   Tarantino et al.[12] extracted plastic-covered vineyards using object-based classification, as mentioned above.   Tarantino et al.[23] also monitored plastic-covered vineyards based on true-color aerial data using an efficient object-based classification approach.   By contrast, the present study focused on object-based classification with an emphasis on testing both the limitations and advantages of fused Landsat-8 data for detecting greenhouses in Xiaoshan District.

2   Materials and methods

2.1   Study area

Xiaoshan District is located in the northeastern region of Hangzhou City, the capital of Zhejiang Province in China, and is the largest center for the growth of flower seedling in the region as well as one of the largest vegetable planting areas.   The region has a subtropical monsoon-type climate with four distinct seasons.

Xiaoshan's economic performance is among the highest of all districts in China.   At the end of 2012, the local GDP reached 161.2 billion Yuan, and the GDP per capita was approximately $17 000.   Figure 1 shows the study area that located in the northeastern of Xiaoshan district, where most of the greenhouses are distributed.   The study area consists of a rectangular experimental area of approximately 77 km^2.
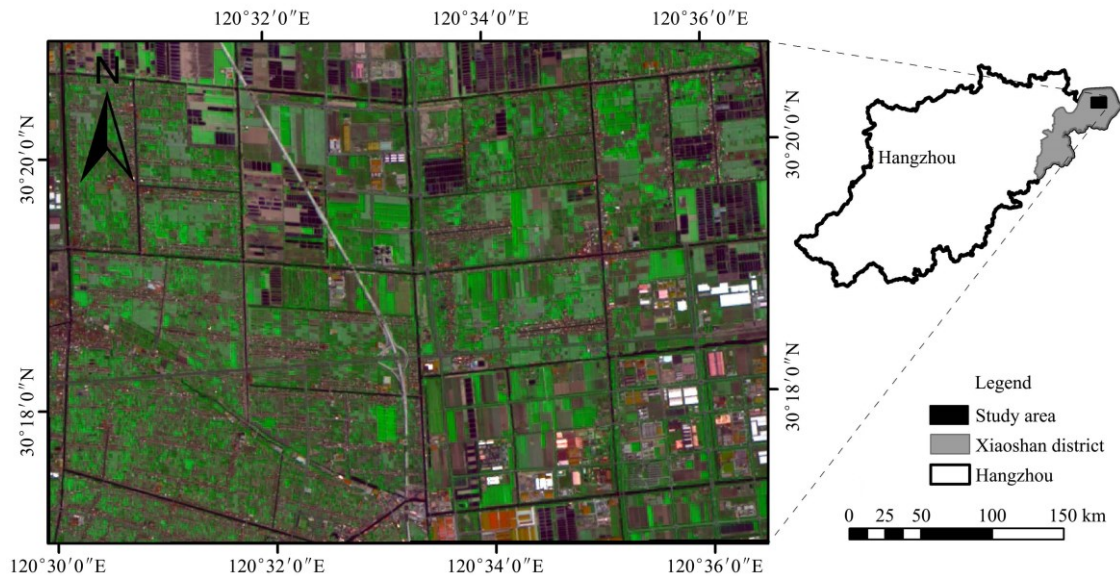

Figure 1   Location of the study area in Hangzhou and the 7-5-4 composition of Landsat-8 satellite imagery

2.2   Experimental design

The objective of this study was to accurately extract greenhouses from Landsat imagery using object-based classification.   We first downloaded an image of Xiaoshan District and preprocessed it to obtain the 15 m fusion image.   Afterward, object-based classification was performed using the eCognition software suite.   Multiple scales were considered to complete the segmentations and the image was divided into different objects at respective suitable scales.   Furthermore, multiple features were used synthetically to improve the accuracy of the segmentation through effective machine learning methods, namely, the random forest (RF) and SVM techniques for object-based feature selection and classification, respectively.   Finally, an accuracy assessment of the classification results was performed through a comparison with the results of the traditional per-pixel SVM classification method.

2.3   Preprocessing of the remote sensing data

The Landsat-8 image remote sensing data were downloaded and geometrically corrected to Universal Transverse Mercator map projection zone 50 with the spheroid and datum of WGS 84.   Panchromatic images with a spatial resolution of 15 m and multispectral images with a spatial resolution of 30 m were acquired on April 14, 2013, with a 16-bit radiometric resolution, as all Operational Land Imager (OLI) and Thermal Infrared Sensor (TIRS) spectral bands were stored as geo-located 16-bit digital numbers[14].   Unlike the Landsat 7 satellite, on which the main imaging instrument was ETM+, Landsat-8 carried two sensors, the OLI and the TIRS.   The OLI offers the following multi-spectral bands: blue (0.45-0.51 μm), green (0.53-0.59 μm), red (0.64-0.67 μm), near-infrared (0.85-0.88 μm), shortwave infrared (1.57-1.65 μm), shortwave infrared (2.11-2.29 μm), and panchromatic (0.50-0.68 μm).   It also recorded in two additional reflective wavelength bands: a new, shorter-wavelength blue band (0.43-0.45 μm) and a new cirrus band (1.36-1.38 μm).   Although the other two thermal bands provided by the TIRS were excluded from

the original bands because of their reduced spatial resolution (100 m), the improvements of the remaining bands in terms of their higher radiometric resolution, narrower spectral wavelength and improved sensor signal-to-noise performance remain attractive. The Landsat-8 scientific team has detailed the promising properties of Landsat-8 in a previous paper[14]. No atmospheric correction of the imagery was performed because there were no clouds or shadows in the study area, and the analysis was performed based on single data. We disregarded the new cirrus band, which was more suitable for cloud detection, and it exhibited serious striping and yielded minimal information in our study.

To acquire better spatial information, one of the most widespread and best performing fusion methods, Gram-Schmidt spectral sharpening, was utilized to fuse the panchromatic and multispectral Landsat-8 satellite images. Both the spectral characteristics of the multispectral image and the spatial resolution of the panchromatic image were successfully preserved, yielding clearer characteristics of greenhouses and other components in the fused image compared with the original multispectral imagery[24].

2.4   Object-based image classification

In this study, object-based classification was implemented using the Definiens® platform.

2.4.1   Image segmentation

Image segmentation is a preliminary step of object-oriented image classification in which the image is divided into homogeneous object primitives. Multi-resolution segmentation, which locally minimizes the average heterogeneity of image objects at a given resolution, was chosen for the segmentation of the study area. The scale parameter is an abstract quantity that determines the maximum allowed heterogeneity for the resulting image objects[25]. A larger scale value produces larger objects, and the inverse also holds. It is advisable that the image objects should be slightly smaller than the real objects, as overly large objects may be more highly subject to error. Once the scale has been determined, three other criteria define the heterogeneity of an object: its color, smoothness, and compactness. The compactness is a function of the object's perimeter

and the number of pixels within the object, whereas the smoothness is a function of the object's perimeter and the perimeter of the object's bounding box; both criteria determine the shape of the object. The shape and color together describe the homogeneity of the object. Researchers have proposed numerous methods for segmentation assessment; however, manual interpretation is generally accepted to be the most accurate method. Tests of a variety of values for each parameter and for various combinations of parameters were conducted to evaluate their impacts on the segmentation accuracy. As a result, the parameters of the multi-resolution segmentation procedure were defined based on a trial-and-error analysis to ensure that the final segmentation matched the visual interpretation. After multiple attempts, we established two different sets of parameter values, as shown in Table 1.

Table 1   Sets of parameter values for two levels of segmentation

	Scale	Shape	Compactness	Num. of objects
L1	200	0.3	0.5	1239
L2	100	0.4	0.6	3175

In this study, we chose a scale value of 200 for the primary level of segmentation, Level 1. A correlation analysis was first conducted to reduce the redundancy of the original bands considered in the segmentation. Because of the high correlations between bands (for instance, the correlation coefficient between bands 1 and 2 was 0.998), the bands were weighted in the two-level segmentation procedure as follows: the weights of bands 2, 4, 5, and 7 were all set to 1, whereas the remaining bands (bands 1, 3, and 6 and the panchromatic band) were given a weight value of 0 and were used only for classification. Segmentation at this level was satisfactory for identifying "large" objects such as paddies, rivers, buildings and plants, as shown in Figure 2. Object features such as NDVI, NDWI and Brightness were calculated to separate the obvious vegetation (NDVI above 0.25), open water (NDWI above -0.054) and light buildings (Brightness above 13500). Because the spectral properties of paddy fields are similar to those of water and our focus was on the classification of greenhouses, paddy fields were simply classified as open

water. As a result of this procedure, the remaining objects, which contained all of the greenhouses in the area, were assigned to the unclassified category for further classification.
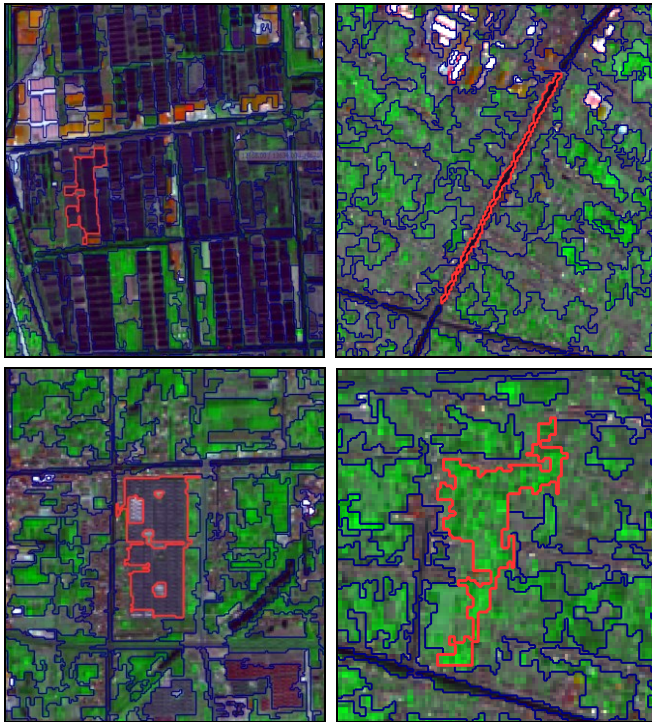

Figure 2   Typical objects obtained via segmentation at Level 1

Different classes are better adapted to different scale levels; therefore, determining the 'best' scale parameter using only one level of segmentation for classification is not advisable. For this reason, Level 2 segmentation was applied to separate greenhouse objects from mixed segments by using a smaller scale value of 100 for finer segmentation within the unclassified category inherited from Level 1. The finer segmentation at Level 2 addressed basic "land use" types – Open Water, Plants, Buildings & Soil, and Greenhouse – among the remaining unclassified objects. The Plants category was further divided into farmland (plants with moderate canopies), dense vegetation (plants with mostly thick canopies), and sparse areas (mostly consisting of plants with the presence of visible ground). Based on the different color properties observed when the image was displayed in 754 band combinations, Buildings & Soil was divided into dull residential, highlighted factory, colorful industrial and road regions. After the segmentation and in reference to the above classification system, 63 objects with strongly characteristic features were chosen as

training samples based on interpretation of the image and on the spatial auto-correlation evident throughout the displayed image.

2.4.2 Feature selection

The object features extracted from a segmented image can potentially be incorporated into further analysis. Determining the most important features significantly contributes to the final classification. Many feature selection methods have been applied in object-based image classification to reduce the dimensionality of the data[26,27]. In addition to the basic spectral information, other attributes can also be utilized in object-based classification, unlike in traditional classification methods. In this study, the spatial relationships between image objects – such as the contrast with respect to neighboring pixels, which measures the difference in contrast between an object and the surrounding area – were incorporated into the object-based image classification. Because a greenhouse is an artificial facility, shape and texture information were also considered in the classification. In total, 53 object features, including the layer values, shape and texture, were considered in this study: (1) customized object features, including the NDVI ((mean layer NIR – mean layer Red)/(mean layer NIR + layer Red)) and NDWI ((mean layer Green – mean layer NIR)/(mean layer Green + mean layer NIR)); (2) the mean value, standard deviation and ratio of each object in all input layers, including 7 fused multi-spectral bands and the panchromatic band; (3) the mean difference from neighbors and contrast with respect to neighboring pixels in all input layers; (4) shape features, including density, length/width and shape indices; and (5) the GLCM, including the homogeneity, contrast, entropy, and second moment, mean and correlation of each object, calculated from the panchromatic band. These features were selected by considering the relationships among the segmented objects and the potential for greenhouses to be discriminated from the other categories based on previous researches[2,16,28]. Details regarding these features can be found in the Reference Book documentation for the software[25].

To determine the effectiveness of the features mentioned above, all features were used to perform

feature selection using one of the most efficacious methods, the RF algorithm in the Waikato Environment for Knowledge Analysis (Weka) system, which was a collection of machine learning algorithms for data mining tasks[29-31]. The RF algorithm is a modern machine learning algorithm developed by Leo Breiman to improve the classification of diverse data. Multiple random trees were constructed by choosing a random number of attributes for each tree without pruning. The most important feature of the RF algorithm is that it estimates the importance of variables according to voting values during the classification process. In this study, a 10-fold cross-validation procedure was implemented within the Weka environment, meaning that 90% of the samples were used for training and the other 10% were used for testing. The number of trees was set to 100, and the number of features required to split the nodes was set to 8 based on the total number of input features[32].

2.4.3 Classification and accuracy assessment

The SVM classification method is a popular nonparametric classification technique with great potential for application in remote sensing[33]. It makes no assumptions about the data distribution and simplifies the number of training samples while providing higher accuracy. In this research, object-based supervised SVM classification was also performed in eCognition Developer 8.7[25].

In remote sensing, classification accuracy refers to the level of agreement between the selected reference materials and the classified data. In total, 294 points were created using the stratified random method to form the error matrix for the 4-category classification results of the applied object-based SVM classification approach. Based on a visual greenhouse analysis of the Landsat-8 satellite imagery, with verification from Google Earth and the high-resolution imagery with the closest temporal match, various accuracy statistics were calculated from the error matrix, including the class producer's accuracy (PA), the class user's accuracy (UA), the overall accuracy (OA), and the overall kappa (OK).

In addition, to assess the area accuracy of the greenhouse classification results, a total greenhouse area of 3.71 km^2 in 104 objects was checked for the following quality indices utilized in previous research[34]:

1) True positive (TP): labeled as greenhouse in both the classification and the manual interpretation.

2) False positive (FP): labeled as greenhouse only in the classification.

3) False negative (FN): labeled as greenhouse only in the manual interpretation.

The following statistics derived from the above three quantities were also considered:

1) Branching factor (BF): FP/TP. Measuring the rate of incorrect greenhouse labeling.

2) Miss factor (MF): FN/TP. Measuring the rate of greenhouse omission.

3) Greenhouse detection percentage (GDP): 100TP/(TP+FP). Measuring the percentage of correct greenhouse categorization achieved by the classification.

4) Quality percentage (QP): 100TP/(TP+FP+FN). Measuring the likelihood of correct classification.

3   Results and discussion

3.1   Feature selection

To select the most appropriate features for Level 2 classification, the RF analysis was conducted prior to the classification. As shown in Table 2, although object features such as texture and shape were expected to be important information in the classification, the feature selection results indicated that spectral properties composed the majority of the most important features. At a finer spatial resolution (such as 1 m), greenhouses could be easily recognized based on their regular shape and texture, but the usefulness of the shape and, especially, the texture information was considerably weakened because mixed pixels were still commonly present in the fused Landsat-8 data as a result of the heterogeneity of the landscape and the limitations imposed by the 15 m spatial resolution of the image. Moreover, because of the small value of the scale parameter used in the segmentation, most objects consisted of small numbers of pixels; therefore, neither the texture features nor the object geometry were particularly distinct[35]. Regarding the neighborhoods surrounding the greenhouses in the study area, most greenhouses are adjacent to farmlands and irrigation

canals and ditches, benefiting from the well-developed water systems in these locations. To facilitate management, these greenhouses are also not far from the residents they serve. As a result, among the most significant features, neighborhood relationships clearly played an important role. However, based on the distribution of all greenhouses, there were no significant unified neighborhood relationships between the greenhouses and the other categories, reflecting the fact that the distribution of most greenhouses was not rigorously planned in the study area. Finally, from the 53 total features, the RF algorithm selected 24 features that yielded a correct classification rate of 0.96 in the Weka system, thereby reducing the number of attributes to be calculated.

Table 2   RF results indicating the most important features in terms of their relevance values

Order	Feature	Relevance value
1	NDVI	2.8
2	Mean diff. from neighbors b5 (0)	1.7
3	Ratio b5	1.7
4	Mean b7	0.9
5	Brightness	0.8
6	Mean diff. from neighbors b2 (0)	0.8
7	NDWI	0.8
8	Mean diff. from neighbors b7 (0)	0.7
9	Contrast with respect to neighboring pixels b5 (3)	0.7
10	Mean diff. from neighbors b6 (0)	0.6
11	Mean diff. from neighbors b1 (0)	0.5
12	GLCM mean p (all dir.)	0.4
13	Mean b4	0.4
14	Mean b5	0.4
15	Ratio b4	0.4
16	Mean b1	0.3
17	Standard deviation b4	0.3
18	Density	0.3

3.2   Image classification

SVM classification, incorporating the features selected in the previous step, was applied to the training samples. The "Linear" kernel implemented in the eCognition software was used.

It was observed that the SVM classification required considerable time when the objects' texture information was included either in the training for feature determination or in the application of the classification procedure.

For comparisons with the results of the object-based classification scheme, the same 7 fused multi-spectral bands and the panchromatic band were stacked to perform per-pixel SVM classification in the ENVI software using the "Linear" kernel.

3.3   Accuracy assessment

The results in Figure 3 reveal that compared with the per-pixel classification map, which exhibits the inevitable salt-and-pepper effect, the object-based classification incorporating different features in addition to the original spectral properties yielded more integrated objects and improved accuracy, in terms of both the total KIA and the OA when compared in Table 3 and Table 4. Furthermore, among the 60 greenhouse test samples, the object-based classification obtained a 100% user's accuracy, whereas 6 sparse vegetation and 1 road region was falsely classified as greenhouse showed in Table 3. As the results shown in Table 4 that exhibit a comparable producer's accuracy with much lower user's accuracy, it further reveals that there is no rigorous spectral discrimination between roads and sparse plants in the study region because they are both covered with low vegetation (perhaps because several roads are located very close to greenbelts). These three categories could be readily confused because of their similar spectral properties showed in Figure 4 for about 50 samples for each classes, as most greenhouses carry vegetation information in April but this information is weakened by the reflection from different covering materials.

Agüera et al.[34] achieved the highest TP value, with a BF of 0.12, an MF of 0.09, a GDP of 91.45 and a QP of 83.49, after applying the Hough transformation for greenhouse discrimination to the best results obtained in multi-spectral image classification; these results were superior to those of all previous studies and are considered as a benchmark for satisfactory performance. From this perspective, the values of the indices presented in Table 5 are of suitable quality compared with other historical results using the same assessment method reported by the author.

A total of 104 objects were selected to compare the correlations between the correct area of each object and its areas as determined via classification and manual identification. The Pearson correlation between the

correct and classification areas in Figure 5a is 0.995, whereas the Pearson correlation between the correct and manual areas in Figure 5b is 0.996; both of these values indicate significant differences at $p<0.05$.
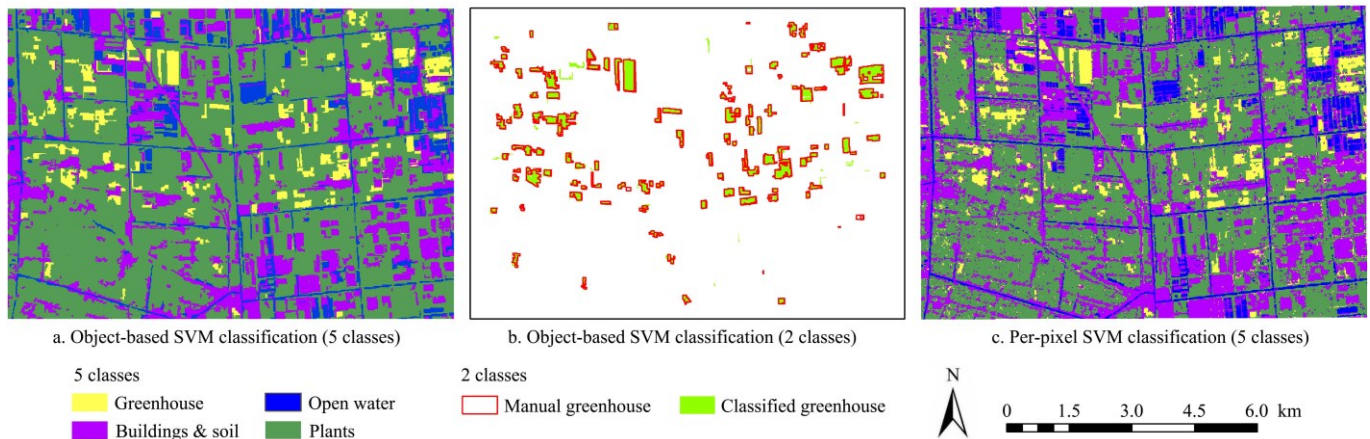

a. Object-based SVM classification (5 classes)   b. Object-based SVM classification (2 classes)   c. Per-pixel SVM classification (5 classes)

5 classes
  Greenhouse   Open water
  Buildings & soil   Plants

2 classes
  Manual greenhouse   Classified greenhouse

N

0   1.5   3.0   4.5   6.0 km

Figure 3   Maps of classification results obtained via object-based classification and per-pixel classification based on the SVM approach

Table 3   Error matrix and accuracy assessment of object-based SVM classification

Classified data/reference	Greenhouse	Open water	Buildings & Soil	Plants	Total	PA	UA
Greenhouse	60	0	0	0	60	89.55%	100.00%
Open Water	0	62	6	1	69	92.54%	89.86%
Buildings & Soil	1	3	64	6	74	91.43%	86.49%
Plants	6	2	0	83	91	92.22%	91.21%
Total	67	67	70	90	294		

Note: Overall classification accuracy = 91.50%, Overall kappa statistic = 0.8859.

Table 4   Error matrix and accuracy assessment of per-pixel SVM classification

Classified data/reference	Greenhouse	Open water	Buildings & Soil	Plants	Total	PA	UA
Greenhouse	52	0	2	6	60	92.86%	86.67%
Open Water	0	44	17	8	69	93.62%	63.77%
Buildings & Soil	1	1	63	9	74	72.41%	85.14%
Plants	3	2	5	81	91	77.88%	89.01%
Total	56	47	87	104	294		

Note: Overall classification accuracy = 81.63%, Overall kappa statistic = 0.7517.

a. Greenhouse spectral information   b. Sparse vegetation spectral information   c. Sparse vegetation spectral information
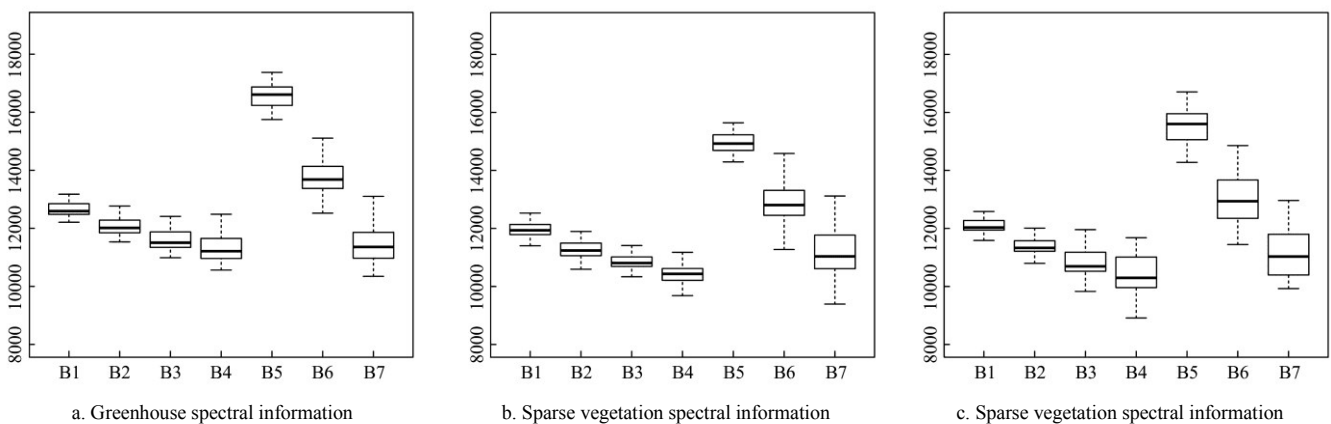
Figure 4   The spectral information of readily confused classes

Table 5   Quality indices for object-based greenhouse classification

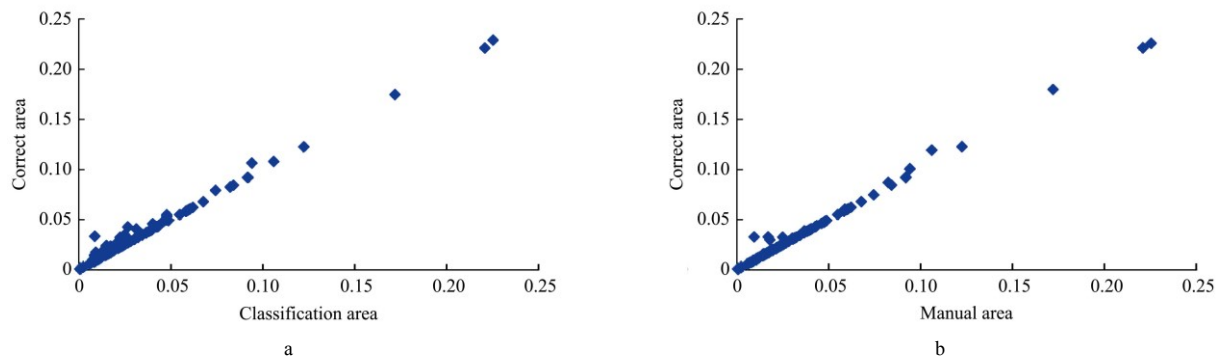| TP/m^2	FN/m^2	FP/m^2	BF	MF	GDP	QP
3616192.76	98416.16	314122.91	0.09	0.02	92.01	89.76

Figure 5   Correlations between the correct object areas and the corresponding classification (a) and manual areas (b)

4   Conclusions

Mapping greenhouses to obtain their accurate distribution and quantity using available remote sensing imagery is not a new task.   Although the accuracy of the final classification is closely related to the performances in major stages of the analysis, including the selection of remote sensing imagery, the generation of the training set, the selection of features, the choice of classifier and the validation based on test samples, different choices and combinations offer their own advantages and disadvantages.   In this study, we focused on object-based classification incorporating features derived from commonly used spectral, texture and spatial information to examine the effect of utilizing the newly available Landsat-8 data to classify greenhouse areas. Because of the complex and varied structures of the targets in the study area, the work was conducted by implementing a two-level object-based classification scheme with a specific emphasis on greenhouses using 15 m fused Landsat-8 data for the northeastern Xiaoshan District of Hangzhou, China.   To distinguish the greenhouse areas from the others, especially the spectrally similar regions of sparse vegetation and roads covered by vegetation, the shape, texture and neighborhood information were all considered to improve the classification accuracy.   We finally obtained a map with an overall accuracy of greater than 85% by investigating different features using the RF algorithm for feature selection prior to SVM classification.   A comparison with the results of traditional per-pixel classification using the same SVM classifier revealed that the object-based classification scheme resulted in significant improvement.   The final greenhouse map demonstrated that Landsat-8 imagery can be satisfactorily used for greenhouse classification by employing a multi-scale object-based classification scheme integrating diverse features.

Many papers have reported that a radial basis function (RBF) kernel is preferred when performing SVM classification; however, we were unable to successfully apply this kernel using the eCognition software. Furthermore, interesting possibilities for future research include incorporating additional texture measures with higher-resolution imagery by combining suitable feature selection methods with SVM classification.

[References]

[1]   Du X M, Wu Z H, Zhang Y Q, Pei X X.   Study on changes of soil salt and nutrient in greenhouse of different planting years. J. Soils Water Conserv., 2007; 2: 019.

[2]   Agüera F, Aguilar F J, Aguilar M A.   Using texture analysis to improve per-pixel classification of very high resolution images for mapping plastic greenhouses.   ISPRS J. Photogrammetry Remote Sens., 2008; 63(6): 635–646.

[3]   Haack B, Bryant N, Adams S.   An assessment of LANDSAT MSS and TM data for urban and near-urban land-cover digital classification.   Remote Sens. Environ., 1987; 21(2): 201–213.

[4]   De Fries R S, Hansen M, Townshend J R G, Sohlberg R. Global land cover classifications at 8 km spatial resolution: the use of training data derived from LANDSAT imagery in decision tree classifiers.   Int. J. Remote Sens., 1998; 19(16): 3141–3168.

[5]   Yuan F, Sawaya K E, Loeffelholz B C, Bauer M E.   Land

cover classification and change analysis of the Twin Cities (Minnesota) Metropolitan area by multitemporal LANDSAT remote sensing.   Remote Sens. Environ., 2005; 98(2–3): 317–328.

[6] Xian G, Homer C, Fry J.   Updating the 2001 National Land Cover Database land cover classification to 2006 by using LANDSAT imagery change detection methods.   Remote Sens. Environ., 2009; 113(6): 1133–1147.

[7] Rodriguez-Galiano V F, Ghimire B, Rogan J, Chica-Olmo M, Rigol-Sanchez J P.   An assessment of the effectiveness of a random forest classifier for land-cover classification.   ISPRS J. Photogrammetry Remote Sens., 2012; 67: 93–104.

[8] Li J, Zhao G X, Li T, Yue Y D.   Study on technique of extracting greenhouse vegetable information from LANDSAT TM image.   J. Soils Water Conserv., 2004; 18(1): 126–129.

[9] Ma Q.   Land use information remote sensing extraction and effects of different land use on soil quality in greenhouse vegetable region.   Master   Dissertation.   Shandong Agricultural University, 2011.

[10] Carvajal F, Agüera F, Aguilar F J, Aguilar M A.   Relationship between atmospheric corrections and training-site strategy with respect to accuracy of greenhouse detection process from very high resolution imagery.   Int. J. Remote Sens., 2010; 31(11): 2977–2994.

[11] Koc-San D.   Evaluation of different classification techniques for the detection of glass and plastic greenhouses from WorldView-2 satellite imagery.   J. Appl. Remote Sens., 2013; 7(1): 073553–073553.

[12] Tarantino E, Aiello A.   Plastic covered vineyard extraction from airborne sensor data with an object-oriented approach. In: Neale C M U, Maltese A, Richter K, ed. Proceedings of SPIE, International Society for Optics and Photonics, 2011; pp. 817415–817415

[13] Agüera F, Liu J G.   Automatic greenhouse delineation from QuickBird and Ikonos satellite images.   Comput. Electron. Agric., 2009; 66(2): 191–200.

[14] Roy D P, Wulder M A, Loveland T R, Woodcock C E, Allen R G, Anderson M C, et al.   LANDSAT-8: science and product vision for terrestrial global change research.   Remote Sens. Environ. 2014; 145: 154–172.

[15] Blaschke T.   Object based image analysis for remote sensing. ISPRS J. Photogrammetry Remote Sens., 2010; 65(1): 2–16.

[16] Han N, Du H, Zhou G, Sun X, Ge H, Xu X.   Object-based classification using SPOT-5 imagery for Moso bamboo forest mapping.   Int. J. Remote Sens, 2014; 35(3): 1126–1142.

[17] Benz U C, Hofmann P, Willhauck G, Lingenfelder I, Heynen M.   Multi-resolution, object-oriented fuzzy analysis of remote sensing data for GIS-ready information.   ISPRS J. Photogrammetry Remote Sens., 2004; 58(3-4): 239–258.

[18] Mitri G H, Gitas I Z.   The development of an object-oriented classification model for operational burned area mapping on the Mediterranean island of Thasos using LANDSAT TM images.   Forest Fire Research & Wildland Fire Safety, 2002: 1–12.

[19] Geneletti D, Gorte B G H.   A method for object-oriented land cover classification combining LANDSAT TM data and aerial photographs.   Int. J. Remote Sens., 2003; 24(6): 1273–1286.

[20] Mitri G H, Gitas I Z.   A semi-automated object-oriented model for burned area mapping in the Mediterranean region using LANDSAT-TM imagery.   Int. J. Wildland Fire, 2004; 13(3): 367–376.

[21] Frohn R C, Reif M, Lane C, Autrey B.   Satellite remote sensing of isolated wetlands using object-oriented classification of LANDSAT-7 data.   Wetlands, 2009; 29(3): 931–941.

[22] Zhu Z, Woodcock C E.   Object-based cloud and cloud shadow detection in LANDSAT imagery.   Remote Sens. Environ., 2012; 118: 83–94.

[23] Tarantino E, Figorito B.   Mapping rural areas with widespread plastic covered vineyards using true color aerial data.   Remote Sens., 2012; 4(12): 1913–1928.

[24] Brower B V, Laben C A.   Process for enhancing the spatial resolution of multispectral imagery using pan-sharpening. Google Patents, 2000.

[25] Imaging D.   eCognition Developer Software: 8.7.1. Reference Book. Raunheim:Trimble Germany GmbH, 2012.

[26] Laliberte A S, Browning D M, Rango A.   A comparison of three feature selection methods for object-based classification of sub-decimeter resolution UltraCam-L imagery.   Int. J. Appl. Earth Observation Geoinformation, 2012; 15: 70–78.

[27] Novack T, Esch T, Kux H, Stilla U.   Machine learning comparison between WorldView-2 and QuickBird-2-simulated imagery regarding object-based urban land cover classification.   Remote Sens., 2011; 3(12): 2263–2282.

[28] Su W, Li J, Chen Y, Liu Z, Zhang J, Low T M et al.   Textural and local spatial statistics for the object-oriented classification of urban areas using high resolution imagery.   Int. J. Remote Sens., 2008; 29(11): 3105–3117.

[29] Gislason P O, Benediktsson J A, Sveinsson J R.   Random forests for land cover classification.   Pattern Recognit. Lett. 2006; 27(4): 294–300.

[30] Breiman L.   Random forests.   Mach. Learn. 2001; 45(1): 5–32.

[31] Livingston F.   Implementing Breiman's Random Forest Algorithm into Weka, 2005.

[32] Löw F, Michel U, Dech S, Conrad C.   Impact of feature selection on the accuracy and spatial uncertainty of per-field crop classification using support vector machines.   ISPRS J. Photogrammetry Remote Sens., 2013; 85: 102–119.

[33] Pal M, Mather P M.   Support vector machines for classification in remote sensing.   Int. J. Remote Sens., 2005; 26(5): 1007–1011.

[34] Agüera F, Aguilar M A, Aguilar F J.   Detecting greenhouse changes from QuickBird imagery on the Mediterranean coast. Int. J. Remote Sens., 2006; 27(21): 4751–4767.

[35] Cai S, Liu D.   A comparison of object-based and contextual pixel-based classifications using high and medium spatial resolution images.   Remote Sens. Lett., 2013; 4(10): 998–1007.